Journal of Solid State Chemistry 182 (2009) 1462–1467

Contents lists available at ScienceDirect

Journal of Solid State Chemistry

journal homepage: www.elsevier.com/locate/jssc

Dispersion control and nematic ordering of Ni/Al layered double hydroxide suspensions

Lingyu Luan, Shangying Liu, Dejun Sun *

Key Laboratory for Colloid and Interface Chemistry of the Ministry of Education, Shandong University, Jinan, Shandong 250100, People's Republic of China

ARTICLE INFO

Article history:
Received 25 December 2008
Received in revised form
3 March 2009
Accepted 7 March 2009
Available online 21 March 2009

Keywords:
Layered double hydroxide (LDH)
Peptization
Isotropic–nematic phase transition
Sol–gel transition

ABSTRACT

In this paper, we report the preparation of aqueous suspensions of Ni/Al layered double hydroxide (LDH) nanoparticles by a non-steady co-precipitation followed by peptization. By choosing suitable peptization temperature and time, well-dispersed suspensions were obtained. Meanwhile, the particle size, shape and size polydispersity can be efficiently controlled. Nematic ordering is observed in colloidal Ni/Al LDH suspensions and confirmed by birefringence observations and SAXS measurements. Furthermore, we showed that the sol–gel transition takes place after a liquid crystalline phase transition in concentrated Ni/Al LDH suspensions. The absence of isotropic–nematic phase separation can be attributed to the fact that the nematic phase droplets are too small to settle to the bottom of the cuvette.

1. Introduction

It is well known that colloidal suspensions can undergo phase transitions which are similar to atomic and molecular systems. For spherical colloids, a disordered fluid phase and an ordered crystal phase can be observed at appropriate colloidal densities. For non-spherical colloids, such as rod- and plate-like particles, intermediate ordered phases between the fluid and crystal can also be observed. For example, the particles exhibit long-range orientational order without long-range positional order (nematic phase, *N*), or with two-dimensional positional ordered (columnar phase, *C*) or one-dimensional positional order (lamellar phase, *L*). In these liquid crystal phases, *I–N* phase transition has been studied for hundred years since suspensions of rod-like vanadium pentoxide and plate-like clay particles were found to exhibit unusual liquid crystal phase behavior [1]. Inspired by these observations, Onsager put forward a theoretical description of *I–N* phase transition in suspensions of such anisotropic colloidal particles. He demonstrated that the driving force for the formation of a nematic phase lies in a gain of excluded volume entropy (favoring the nematic state) compensating a loss of orientational entropy (favoring the isotropic state) [2]. Furthermore, he addressed that the particle shape alone is enough to induce *I–N* phase transition, and thus hard rods or plates without any interactions may form a nematic phase [3]. This has been confirmed by computer simulation [4]. *I–N* phase transition in suspensions of rod-like particles has been studied extensively for many decades in experiments, theory and simulations [5–7]. However, for suspensions of colloidal platelets, the *I–N* phase transition is almost always obscured in the interference of gelation [8–10], so it is natural to focus on other systems of inorganic platelets. In recent years, suitable experimental model systems of approximately hard colloidal platelets have been developed [11–13]. Concentrated suspensions of $Ni(OH)_2$ platelets showed *I–C* transition but not *I–N* transition. The absence of a nematic phase can be attributed to the much lower aspect ratio (diameter to thickness). While suspensions of gibbsite platelets with a higher aspect ratio and a slightly higher polydispersity showed the full range of liquid crystal phase transitions predicted for hard platelets, i.e., *I–N* and *N–C* phase transitions. However, these investigations were not related to the colloidal domain of layered double hydroxide (LDH).

Layered double hydroxides are a class of inorganic compounds with the general formula $[M^{2+}_{1-x}M^{3+}_{x}(OH)_2]^{x+}A^{n-}_{x/n}\cdot mH_2O$, where M^{2+} and M^{3+} are di- and tri-valent metal cations, such as Mg^{2+}, Co^{2+}, Ni^{2+}, Al^{3+}, Fe^{3+}, Cr^{3+}, etc., and x changes with M^{2+}/M^{3+} molar ratio of preparation. Structurally, LDHs can be characterized as containing brucite-like layers, where some divalent metal cations have been partially substituted by trivalent metal cations (isomorphic substitution) to form positively charged sheets. The surface charge can be tuned by varying the ratio of M^{2+}/M^{3+} and it is compensated by exchangeable anions and water molecules in the interlayers [14,15]. Such structural characteristics and compositional variability makes LDHs have potential applications in wide areas, such as catalysts, catalyst supports and nanocomposites [16,17]. In our previous work, Mg/Al LDH suspensions have

* Corresponding author. Tel.: +86 531 88364749; fax: +86 531 88365437.
E-mail address: djsun@sdu.edu.cn (D. Sun).

0022-4596/$ - see front matter © 2009 Elsevier Inc. All rights reserved.
doi:10.1016/j.jssc.2009.03.006

been investigated for their stability [18], rheological properties [19–21] and the ability to stabilize Pickering emulsions [22,23]. And recently, *I–L* phase transition was found in $Mg^{2+}/Al^{3+} = 1:1$ LDH suspensions, while *I–N* phase transition was found in $Mg^{2+}/Al^{3+} = 2:1$ LDH suspensions [24–26]. To the best of our knowledge, no same kinds of liquid crystal phase transitions in Ni/Al LDH suspensions have been reported yet. Michot et al. synthesized takovites containing different anions, as a result of the poorly defined particle morphologies and some degree of aggregation, they only observed a sol–gel transition rather than a liquid crystal phase transition [27]. In order to study the liquid crystal phase transition in Ni/Al LDH suspensions, well-dispersed and transparent suspensions with well-defined particles and acceptable particle size polydispersity but without particle aggregation are needed.

Up to now, there have been many reports on the synthesizing of LDHs. Non-steady co-precipitation [28–31], co-precipitation of mixed salt solutions at varied or constant pH, followed by peptizing at a certain temperature, has been successfully used to synthesize LDHs. Our group has reported that co-precipitating Mg^{2+}/Al^{3+} (2:1) in $NH_3 \cdots H_2O$ solution at pH 9.5 and then peptizing the obtained precipitate at 80 °C for 24 h results in well-dispersed colloidal LDH suspensions [24–26]. Zhao et al. prepared Mg/Al-carbonate LDH nanoparticles with uniform crystalline size using a rapid mixing and nucleation process in a colloid mill followed by a separate aging process [32]. Xu et al. reported a fast co-precipitation followed by controlled hydrothermal treatment to prepare stable homogeneous suspensions of monodispersed Mg/Al LDH nanoparticles [33]. In this paper, we report a simple and convenient synthesis method based on non-steady co-precipitation followed by hydrothermal treatment to prepare colloidal Ni/Al LDH nanoparticles in aqueous suspensions. By choosing the peptization temperature and time, we can efficiently control the particle size, shape and size distribution, and finally obtain well-dispersed suspensions. What is more, nematic ordering is observed in concentrated Ni/Al LDH aqueous suspensions and confirmed by birefringence observations and SAXS measurements.

2. Experimental

2.1. Preparation of Ni/Al LDH suspensions

We have investigated the peptization behavior of Ni/Al LDH aggregates with different Ni/Al molar ratio, however, under the peptization conditions adopted in this study, they cannot be well dispersed to form the required sols for the investigation of liquid crystal phase transitions in Ni/Al LDH suspensions. Comparing all the obtained suspensions, we choose the Ni/Al molar ratio of 1:1.

Generally, to prepare stable suspensions of Ni/Al LDH, 350 ml diluted $NH_3 \cdot H_2O$ solution (3.0 M) was quickly added into 600 ml mixed aqueous solution of $NiCl_2 \cdot 6H_2O$ and $AlCl_3 \cdot 6H_2O$ (total metal concentration 0.3 M, Ni/Al molar ratio 1:1) under vigorous stirring. The final pH value of the suspension was about 9.8. The obtained precipitate was aged in air at room temperature with stirring for 45 min. After filtration, the filter cake was washed thoroughly with deionized water, then collected, redispersed in deionized water and placed in an autoclave for peptization at different temperatures for different times. A part of each suspension was dried for subsequent XRD analysis, and the rest was kept in suspension under a nitrogen atmosphere to prevent acidification by dissolved CO_2 for TEM, size distribution and rheology measurement. The samples used for birefringence observations and SAXS measurement were prepared as follows. After peptization at 130 °C for 24 h, the obtained sol was concentrated by vacuum distillation until the particle concentration reached 22 wt%, then the concentrated sample was kept in a closed flask under a nitrogen atmosphere to prevent acidification by dissolved CO_2. The suspensions of different concentrations were prepared by diluting the concentrated suspension of 22 wt%, and then closed in flat cuvettes with 1 mm slit widths and capillaries, respectively.

2.2. Characteristic methods

Powder X-ray diffraction (XRD) patterns were collected using a Ringku D/MAX-rA X-ray diffractometer with Cu $K\alpha$ radiation ($\lambda = 1.54184$ Å). Infrared spectra were collected on a VERTEX-70 FTIR after 40 scans within 4000–370 cm^{-1} at a resolution of 4 cm^{-1} by measuring the IR absorbance of a KBr disk containing 1–2 wt% of the Ni/Al LDH sample. The transmission electron micrographs (TEM) were obtained on a JEM-2100 electron microscope operated at 200 KV. For TEM observations, the suspensions were diluted with deionized water and ultrasonic treatment for 10 min, and then deposited on carbon-coated copper grids. The particle size distributions and zeta potential were both measured with a Malvern Zetasizer 3000. The rheology measurements were performed on a HAKKE RS75 Rheometer with a coaxial cylinder sensor system (Z41 Ti). The viscosity curves were collected with shear rate ranging from 0 to 1000 s^{-1}. For oscillatory measurements, the amplitude of the applied stress was chosen in the linear viscoelastic regimes and the data were recorded in the range of frequency between 0.01 and 100 Hz. The macroscopic phase behavior of Ni/Al LDH suspensions was observed between crossed polarizers. The small angle X-ray scattering (SAXS) measurements were performed at Beijing Synchrotron Radiation Facility (BSRF). The radiation is fixed at 0.154 nm and the distance from the sample to detector is 1.6 m.

3. Results and discussion

3.1. Effect of peptization temperature on particle size

The XRD patterns of Ni/Al LDH obtained under different peptization temperature for 24 h are presented in Fig. 1. Whatever the peptization temperature is, all the samples have

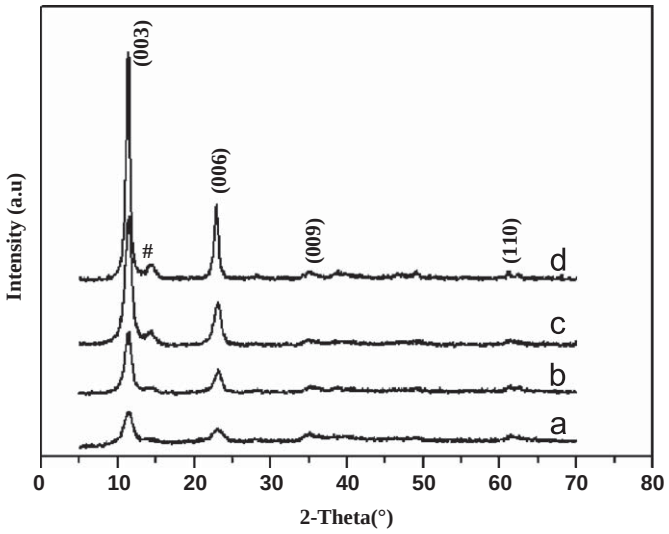

Fig. 1. X-ray diffraction patterns of dried powders of Ni/Al LDH suspensions peptized at different temperatures for 24 h: (a) 80 °C; (b) 100 °C; (c) 130 °C; and (d) 150 °C.

three sharp diffraction peaks close to $2\theta = 11^\circ$, 24°, 35°, corresponding to the diffraction planes (003), (006) and (009) located at 7.6, 3.8 and 2.6 Å, respectively, typical of hydrotalcite-like compounds. According to the basal spacing data, we can infer that carbonate ions do not intercalate into the interlayer. The peak marked # represents the formation of AlO(OH). The absence of (01*l*) reflections indicates that the samples have a high stacking fault density [34]. It can be also seen that the intensity of the peak is increased and the full width at half maximum is decreased with the increasing of the peptization temperature. These indicate that the samples crystallinity is improved by enhancing the peptization temperature.

FTIR spectra of Ni/Al LDH powders peptized at different temperatures for 24 h are shown in Fig. 2. Both samples are typical Ni/Al-Cl LDH peaks including a broad band at 3450 cm^{-1} (υ_{OH}), a rather weak peak at 1365 cm^{-1} (due to CO_3^{2-} converted from CO_2 captured from air), a peak at 1625 cm^{-1} (δ_{H_2O}) and bands at 680 and 447 cm^{-1} (M–O vibration and M–O–H bending) [35–37].

The morphologies of Ni/Al LDH nanoparticles of the suspensions peptized at different temperatures for 24 h are shown in Fig. 3, and the particle sizes given by size distribution are listed in Table 1. Apparently, the particles are all roughly hexagonal plate-like in shape. At the lowest peptization temperature, 80 °C (Fig. 3a), the suspensions are not fully peptized and the particles distinctly aggregate. The smaller particles are well defined with particle size ranging from 10 to 30 nm while the larger aggregates with size over than 1 μm (Table 1). When the peptization temperature is up to 100 °C (Fig. 3b), the particles become larger but inhomogeneous. Particle polydispersity increases and there is still some degree of aggregation. After peptization at 130 °C (Fig. 3c), the particles exhibit a well-defined hexagonal shape with the size in the range of 15–30 nm, forming a roughly monodispersed suspension. When the temperature is raised to 150 °C, the particles become much larger and thicker, but they are much closer to discoid in shape (Fig. 3d). Size distribution measured by the Zetasizer3000 gave similar results to TEM observations (Fig. 4a). As the size distribution gives the hydrodynamic diameter so the value is bigger than the real corner to corner dimension of Ni/Al LDH particles in TEM images. For a peptization temperature of 100 °C, the particle size distribution curves show one broad peak, indicating a higher particle polydispersity in these suspensions. While the curve for the suspensions peptized at 130 °C has only one sharp peak with an average diameter of 86 nm. This reveals that 100 °C is not high enough to fully disperse the aggregates. As the peptization temperature is up to 150 °C, the curve shows two broad peaks again, implying the increasing of particle polydispersity due to reaggregation of larger particles. Comparing all the obtained suspensions, we determined 130 °C to be the optimal peptization temperature.

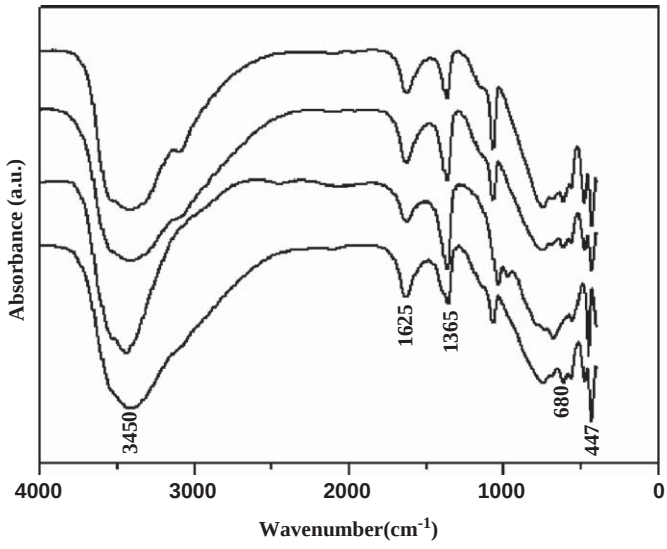

Fig. 2. FTIR spectra of dried powders of Ni/Al LDH suspensions peptized at different temperatures for 24 h: (a) 80 °C; (b) 100 °C; (c) 130 °C; and (d) 150 °C.

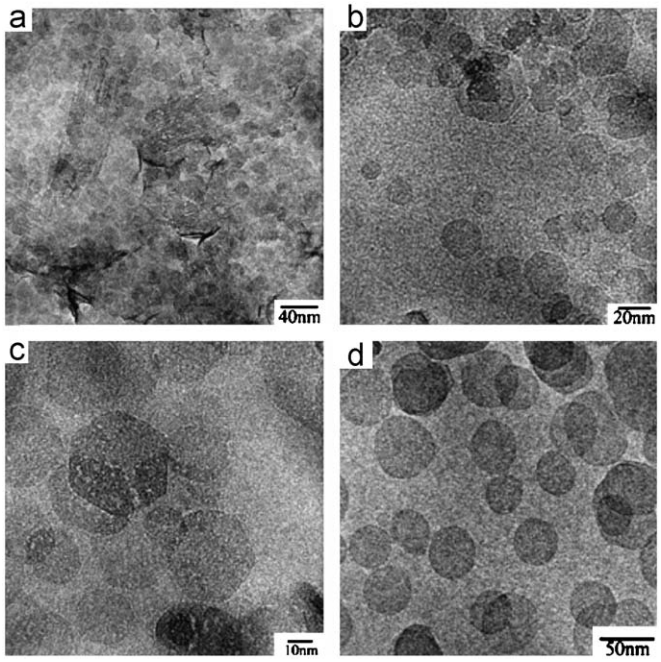

Fig. 3. TEM images of Ni/Al LDH nanoparticles of the suspensions peptized at different temperatures for 24 h: (a) 80 °C; (b) 100 °C; (c) 130 °C; and (d) 150 °C.

Table 1
Ni/Al LDH particle sizes (nm) under different peptization conditions.

Time (h)	80 °C	100 °C	130 °C	150 °C
12	×	×	44.9[a] 145.1[b]	72.6
16	×	167.3	124.7	129.5
24	80.7[a] 1129.3[b]	117.3	86	71.6[a] 188.4[b]
48	354.9	129.0	125.3	160

Note: "×" such peptization condition produces flocculated sample.
[a] The peak value of smaller particles.
[b] The peak value of larger particles that are not dispersed or reaggregated. Both of them are calculated from the particle size distribution, which are bigger than the real corner to corner dimension of LDH particles from TEM images.

3.2. Effect of peptization time on particle size

Not only the peptization temperature but also the peptization time has a significant effect on the stability and dispersibility of the obtained colloidal suspensions. Fig. 5a–c and Table 1 show the morphologies and sizes of Ni/Al LDH nanoparticles of the suspensions peptized at 130 °C for different times, respectively, and the corresponding particle size distribution is presented in Fig. 4b. For a short peptization time (12 h), large and small particles are both observed and the particle polydispersity is higher (Fig. 5a), so the particle size distribution curve has two sharp peaks. As the peptization time is prolonged to 24 h (Fig. 5b),

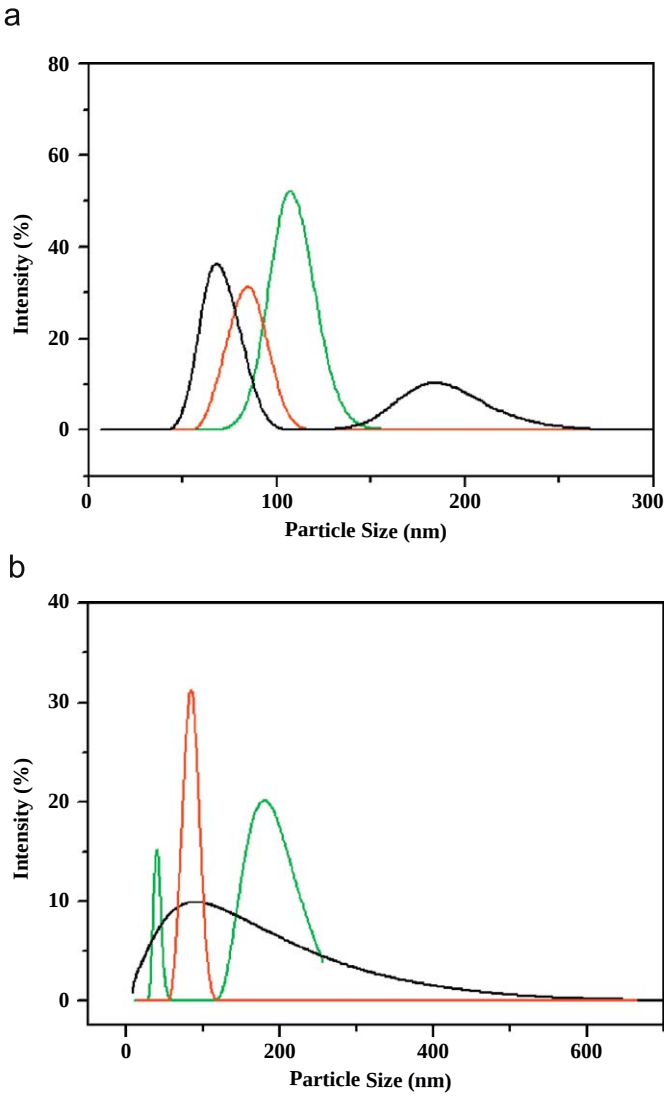

Fig. 4. Size distribution curves of Ni/Al LDH particles: (a) peptization at different temperatures for 24 h and (b) peptization at 130 °C for different times.

the particles grow larger and become relatively homogeneous. The particle size distribution curve shows one sharp, narrow peak, indicating a lower size polydispersity. However, when the peptization time is up to 48 h (Fig. 5c), the curve shows a much broader peak because more particles reassemble into larger aggregates. Therefore, we considered that the optimal peptization time was 24 h. The chemical composition of the Ni/Al LDH obtained at 130 °C for 24 h was probed by EDS analysis (Energy Dispersion Spectrometer) and shown in Fig. 5d, which indicates the presence of Ni, Al, Cl and O, and gives the mole ratio of Ni/Al = 1, equaling the initial designed value (1.0). The presence of C and Cu are derived from the copper grids used in the TEM experiment. Therefore, the chemical composition of the Ni/Al LDH is $Ni_{0.50}Al_{0.47}(OH)_2Cl_{0.47}\cdot 0.71H_2O$. The zeta potential of the Ni/Al LDH nanoparticles measured with Malvern Zetasizer 3000 was about +60 mV at $4 \leqslant pH \leqslant 6$.

3.3. Dispersibility and growth of Ni/Al LDH particles

In our group, well-dispersed Mg/Al LDH suspensions can be prepared by peptization at 80 °C for 24 h. However, such lower peptization temperature cannot make the initial amorphous Ni/Al

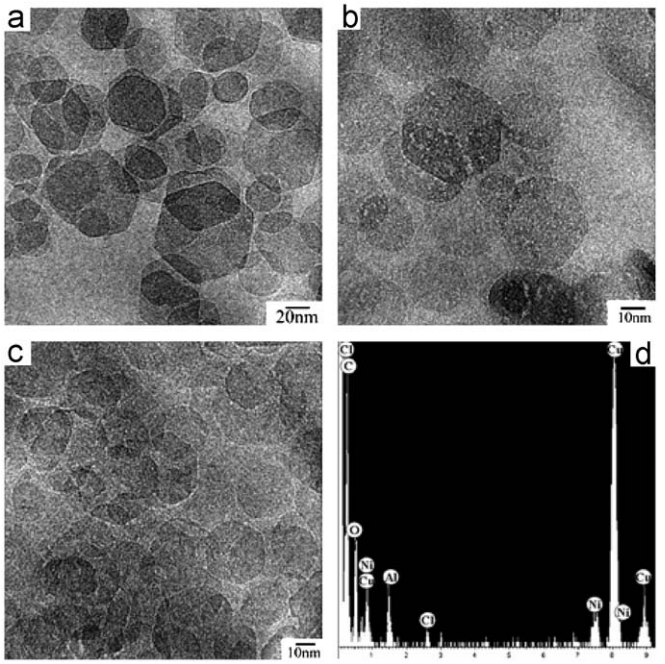

Fig. 5. TEM images of Ni/Al LDH nanoparticles of the suspensions peptized at 130 °C for: (a) 12 h; (b) 24 h; (c) 48 h; and (d) chemical compositions analyzed with EDS (Energy Dispersion Spectrometer).

LDH materials disperse and gives rise to flocculated samples (" × " in Table 1), unsuitable for the investigation of liquid crystal phase transition in Ni/Al LDH suspensions. This indicates that Mg/Al LDH is easy to disperse in aqueous solution, while Ni/Al LDH prefers to aggregate in aqueous solution, so the necessary condition to obtain a well-defined sol is to enhance the dispersibility by increasing the peptization temperature and time, which is a prerequisite for the crystal growth mechanism of dissolution and recrystallization. Generally speaking, under hydrothermal conditions, particle growth mechanisms follow Ostwald ripening, namely, the smaller and larger particles have different surface free energies, resulting in the dissolution of smaller particles and the growth of larger particles. For lower hydrothermal temperatures (80 and 100 °C) or shorter peptization times (12 and 16 h), the solubility of the particles is reduced, leading to much smaller particles, and thus the suspensions are not well dispersed because of the strong attraction between the particles and the glue effect of amorphous LDH materials. For moderate peptization temperatures (130 °C) or times (24 h), the particle growth undergoes dissolution and recrystallization, thus producing larger and homogeneous particles. However, when peptized at higher temperatures (150 °C) or longer times (48 h), much larger particles are obtained, where edge-to-surface interactions dominated to form larger aggregates, so the suspensions are unstable [38].

The dispersibility of the Ni/Al LDH suspensions was also characterized by viscosity measurements. As shown in Fig. 6, the suspensions are all shear-thinning and the unpeptized suspension has the highest viscosity. The viscosity decreased with the peptization temperature. Notably, the viscosity of the suspension peptized at 80 °C is almost equal to that of the unpeptized suspension. This indicates lower temperatures are not enough to completely disperse the amorphous Ni/Al LDH aggregates, while the suspensions peptized at higher temperatures are well dispersed and have low viscosity. That is to say, in the initial stage of hydrothermal treatment, the particles firstly experience disaggregation, and then the growth of the LDH individual

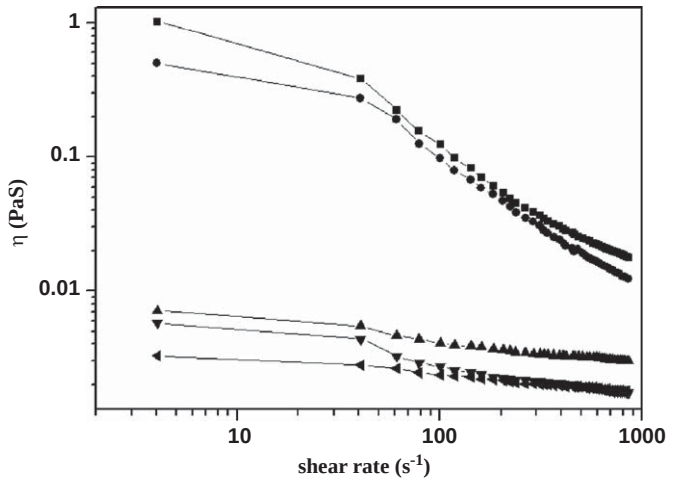

Fig. 6. Viscosity curves of Ni/Al-LDH suspensions unpeptized and peptized at different temperatures for 24 h. The concentrations of these suspensions are all 5 wt% (■: unpeptized; ●: 80 °C; ▲: 100 °C; ▼: 130 °C; and ◀: 150 °C).

crystallites takes place via Ostwald ripening. On the other hand, the particles' Brownian motion is enhanced under hydrothermal treatment, so the particles on the aggregate surface overcome the interparticle interaction through collision and escape from the aggregate, and hence they will stably suspend in the suspension because of the strong electrostatic repulsive forces. These are the possible reasons that peptization at 80 °C for 24 h can only partly disperse the Ni/Al LDH aggregates. The disaggregation of the amorphous LDH is completed after peptization at 100 °C, and then the particle growth via the following processes [33,39]. Small crystallites dissolve and the Mg and Al species deposit onto the bigger crystallites. Meanwhile, the cations diffuse within the hydroxide layers to reduce the lattice defect and form a better crystallized LDH particle. However, the continuous growth makes the particles become much larger. These larger particles may overcome the electrostatic repulsive forces and aggregate again. The change in particle morphologies from hexagonal to discoid when the peptization temperature is up to 150 °C can be attributed to the fact that the increasing of peptization temperature may affect the processes of dissolution, deposition and diffusion during the particle growth. In conclusion, stable and monodispersed suspensions of Ni/Al LDH nanoparticles with well-defined morphologies were obtained at the optimal conditions of peptization temperature 130 °C and time 24 h. So the Ni/Al LDH suspensions used in the following birefringence observations, SAXS and rheology measurements were obtained under these hydrothermal conditions.

3.4. Phase behavior of Ni/Al LDH suspensions

In our previous reports of Mg/Al LDH suspensions, an isotropic–lamellar (*I–L*) and an isotropic–nematic (*I–N*) phase transition was found in $Mg^{2+}/Al^{3+} = 1{:}1$ and $Mg^{2+}/Al^{3+} = 2{:}1$ LDH suspensions, respectively [24–26]. Ni/Al LDH particles are also anisotropic, according to Onsager theory, a liquid crystalline phase transition may occur in such suspensions at high enough particle concentrations. As expected, when observed between crossed polarizers (Fig. 7), the Ni/Al LDH suspensions with concentrations lower than 8 wt% are completely isotropic (Fig. 7a), while suspensions with higher concentrations show permanent birefringence, and the relative amount of the birefringent phase increases with particle concentrations (Fig. 7b–d). The phase structure of the birefringent phase was further characterized by small angle X-ray scattering (SAXS) measurements. SAXS is a useful technique for the investigation of liquid crystal systems and it can distinguish various liquid-crystalline phases depending on different scattering patterns or curves. As shown in Fig. 8, the inset pictures are original SAXS pattern (a) and birefringence (b) of the Ni/Al LDH suspension with a concentration of 14 wt%. SAXS measurements show that its scattering is typical for a nematic phase [40].

However, after a longer resting time of 4 months, the suspensions only show nematic ordering and no isotropic–nematic phase separation is observed. This seems quite similar to aqueous clay suspensions, where gelation takes place before isotropic–nematic phase separation [8]. That is to say, in Ni/Al LDH suspensions the isotropic–nematic phase separation may be prevented by gelation, so we made oscillatory measurements on concentrated Ni/Al LDH suspensions and the storage (elastic) modulus G' and loss modulus G'' of the systems were determined. As shown in Fig. 9, for a Ni/Al LDH suspension with a concentration of 14 wt%, G' is lower than G'' and the suspension is slightly viscous, typical of a sol. However, the opposite is observed in the 17 wt% suspension, where G' is markedly higher

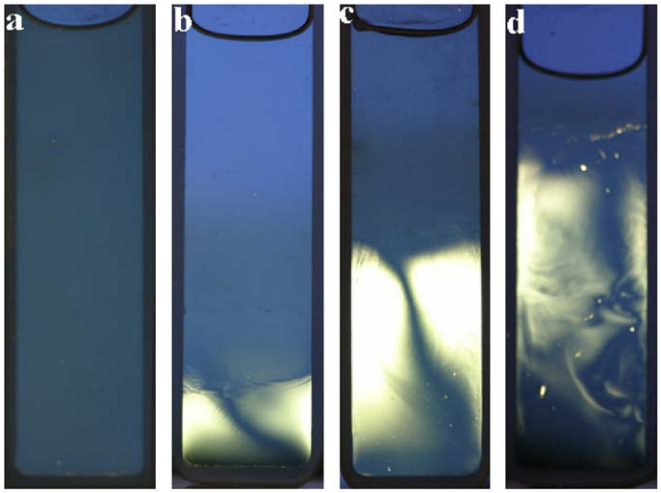

Fig. 7. Phase behavior of Ni/Al LDH suspensions with different concentrations as observed between crossed polarizers after a resting time of 4 months: (a) 8 wt%; (b) 11 wt%; (c) 14 wt%; and (d) 17 wt%.

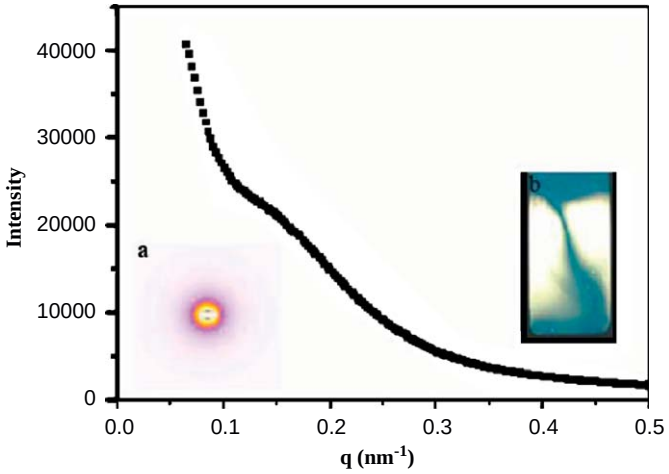

Fig. 8. Small angle X-ray scattering curve of Ni/Al LDH suspension with a concentration of 14 wt%. The inset pictures are original SAXS pattern (a) and birefringence of the suspension (b).

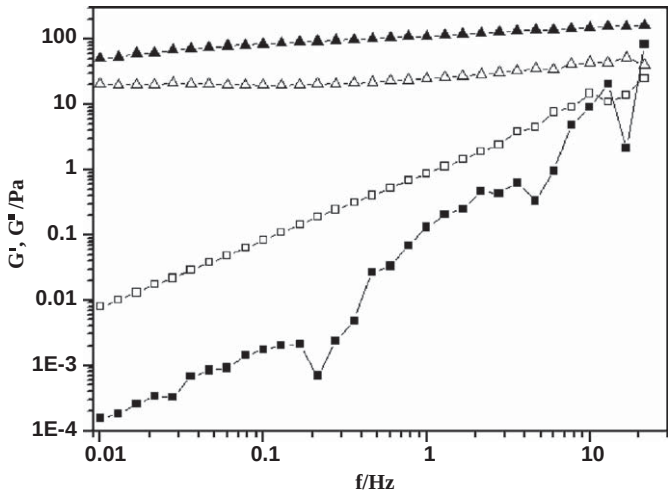

Fig. 9. G' and G'' as a function of frequency at a constant stress (0.3 Pa) for Ni/Al LDH suspensions with different concentrations (■, □: 14 wt% and ▲, □: 17 wt%. Full symbols: storage modulus G' and open symbols: loss modulus G'').

than G'' and both of them do not vary much within the examined frequencies, which reveals the formation of a gel. So we can conclude that the sol–gel transition takes place after a liquid crystalline phase transition in Ni/Al LDH suspensions. Therefore, the phase behavior of Ni/Al LDH suspensions can be explained as follows. In a nematic sol sample, the Ni/Al LDH particles are much smaller than Mg/Al LDH particles (120 nm), and the formed nematic droplets are too small to settle to the bottom of the cuvette. They suspend throughout the whole suspension, so no sharp phase boundary and no isotropic–nematic phase separation is observed. The broad peak on the SAXS curve reflects a surface-to-surface interaction between neighboring particles [40]. This indicates that a so-called repulsive gel, stabilized by electrostatic repulsive forces between the electrical double layers of the particles, can form in Ni/Al LDH suspensions.

4. Conclusion

In summary, by suitable choice of peptization temperature and time, aqueous suspensions of Ni/Al LDH nanoparticles were successfully prepared with controlled morphologies and size distribution, which are important for the formation of oriented films, liquid crystal phase behavior and the stability of Pickering emulsions. The optimal conditions for synthesizing stable and monodispersed suspensions of hexagonal Ni/Al LDH nanoparticles are peptization at 130 °C for 24 h. Nematic ordering without isotropic–nematic phase separation is observed in their concentrated suspensions. This can be attributed to the fact that the nematic phase droplets are too small to settle to the bottom of the cuvette. Due to the permanent positive surface charge of Ni/Al LDH particles, these suspensions may respond to an external magnetic field and an AC electric field. In our future investigation, we plan to investigate the magnetic and electric field-induced birefringence which could be interesting for applications in simple display devices.

Acknowledgments

We acknowledge the financial support from the National Nature Science Foundation of China (20603020), Doctoral Programs Foundation of Ministry of Education of China (20060422021). We thank Prof. Xusheng Feng for helpful discussions and Prof. Pamela Holt (Shandong University) for assistance in editing the manuscript's English.

References

[1] I. Langmuir, J. Chem. Phys. 6 (1938) 873–896.
[2] L. Onsager, Ann. NY Acad. Sci. 51 (1949) 627–659.
[3] D. van der Beek, H.N.W. Lekkerkerker, Langmuir 20 (2004) 8582–8586.
[4] M.A. Bates, J. Chem. Phys. 111 (1999) 1732–1736.
[5] M.P.B. van Bruggen, J.K.G. Dhont, H.N.W. Lekkerkerker, Macromolecules 32 (1999) 2256–2264.
[6] G.J. Vroege, H.N.W. Lekkerkerker, Rep. Prog. Phys. 55 (1992) 1241–1309.
[7] P. Bolhuis, D. Frenkel, J. Chem. Phys. 106 (1997) 666–687.
[8] J-C.P. Gabriel, C. Sanchez, P. Davidson, J. Phys. Chem. 100 (1996) 11114–11139.
[9] A. Mourchid, A. Delville, J. Lambard, E. Lecolier, P. Levitz, Langmuir 11 (1995) 1942–1950.
[10] A. Mourchid, E. Lécolier, H. Van Damme, P. Levitz, Langmuir 14 (1998) 4718–4723.
[11] F.M. van der Kooij, K. Kassapidou, H.N.W. Lekkerkerker, Nature 406 (2000) 868–871.
[12] D. van der Beek, H.N.W. Lekkerkerker, Europhys. Lett. 61 (2003) 702–707.
[13] A.B.D. Brown, S.M. Clarke, A.R. Rennie, Langmuir 14 (1998) 3129–3132.
[14] F. Cavani, F. Trifiro, A. Vaccari, Catal. Today 11 (1991) 173–301.
[15] V. Rives (Ed.), Layered Double Hydroxides: Present and Future, Nova Science Publishers, New York, 2001.
[16] H.C. Greenwell, S. Stackhouse, P.V. Coveney, W. Jones, J. Phys. Chem. B 107 (2003) 3476–3485.
[17] S.P. Newman, S.J. Williams, P.V. Coveney, W. Jones, J. Phys. Chem. B 102 (1998) 6710–6719.
[18] X.J. Wang, D.J. Sun, S.Y. Liu, R. Wang, J. Colloid Interface Sci. 289 (2005) 410–418.
[19] S.P. Li, W.G. Hou, D.J. Sun, P.Z. Guo, C.X. Jia, J.F. Hu, Langmuir 19 (2003) 3172–3177.
[20] S.P. Li, W.G. Hou, J.C. Xiao, J.F. Hu, D.Q. Li, Colloids Surf. A 224 (2003) 149–156.
[21] S.P. Li, W.G. Hou, J.F. Hu, D.Q. Li. J. Dispers, Sci. Technol. 24 (2003) 145–152.
[22] F. Yang, S. Liu, J. Xu, Q. Lan, F. Wei, D.J. Sun, J. Colloid Interface Sci. 302 (2006) 159–169.
[23] F. Yang, Q. Niu, Q. Lan, D. Sun, J. Colloid Interface Sci. 306 (2007) 285–295.
[24] S.Y. Liu, J. Zhang, N. Wang, W.R. Liu, C.G. Zhang, D.J. Sun, Chem. Mater. 15 (2003) 3240–3241.
[25] N. Wang, S.Y. Liu, J. Zhang, Z.H. Wu, J. Chen, D.J. Sun, Soft Matter 1 (2005) 428–430.
[26] J. Zhang, L.Y. Luan, W.X. Zhu, S.Y. Liu, D.J. Sun, Langmuir 23 (2007) 5331–5337.
[27] L.J. Michot, J. Ghanbaja, V. Tirtaatmadja, P.J. Scales, Langmuir 17 (2001) 2100–2105.
[28] S.H. Han, W.G. Hou, C.G. Zhang, D.J. Sun, X.R. Huang, G.T. Wang, J. Chem. Soc. Faraday Trans. 94 (1998) 915–918.
[29] P.Z. Guo, D.J. Sun, J. Zhang, C.G. Zhang, Chem. Lett. 32 (2003) 250–251.
[30] G. Lagaly, O. Mecking, D. Penner, Colloid Polym. Sci. 279 (2001) 1090–1096.
[31] E. Gardner, K.M. Huntoon, T.J. Pinnavaia, Adv. Mater. 13 (2001) 1263–1266.
[32] Y. Zhao, F. Li, R. Zhang, D.G. Evans, X. Duan, Chem. Mater. 14 (2002) 4286–4291.
[33] Z.P. Xu, G. Stevenson, C.Q. Lu, G.Q. Lu, J. Phys. Chem. B 110 (2006) 16923–16929.
[34] M. Bellotto, B. Rebours, O. Clause, J. Lynch, D. Bazin, E. Elkaim, J. Phys. Chem. 100 (1996) 8527–8534.
[35] M.J. Hernandez-Moreno, M.A. Ulibarri, J.L. Rendon, C. Serna, J. Phys. Chem. Miner. 12 (1985) 34–38.
[36] Z.P. Xu, G.S. Stevenson, C.Q. Lu, G.Q. Lu, P.F. Bartlett, P.P. Gray, J. Am. Chem. Soc. 128 (2006) 36–37.
[37] Z.P. Xu, H.C. Zeng, J. Phys. Chem. B 105 (2001) 1743–1749.
[38] J.A. Gursky, S.D. Blough, C. Luna, C. Gomez, A.N. Luevano, E.A. Gardner, J. Am. Chem. Soc. 128 (2006) 8376–8377.
[39] Z.P. Xu, G.Q. Lu, Chem. Mater. 17 (2005) 1055–1062.
[40] A.V. Petukhov, D. van der Beek, R.P.A. Dullens, I.P. Dolbnya, G.J. Vroege, H.N.W. Lekkerkerker, Phys. Rev. Lett. 95 (2005) 077801–077804.